Anharmonic lifetimes of low-frequency optical phonons in LaF_3 with the use of monoenergetic generation and detection

R. S. Meltzer and J. E. Rives
Department of Physics and Astronomy, University of Georgia, Athens, Georgia 30602

G. S. Dixon
Department of Physics, Oklahoma State University, Stillwater, Oklahoma 74078
(Received 25 April 1983)

Dynamics of large-$\vec{k}$ acoustic phonons and low-frequency optical phonons in LaF_3 are investigated. Monoenergetic nonequilibrium phonons are obtained by electron-phonon relaxation of laser-excited Er^{3+} ions and are detected with phonon-induced absorption of the anti-Stokes vibronic sideband of the $^3P_0$ state of Pr^{3+}. Monoenergetic phonon occupation numbers of 10^{-2} are observed and the decay of these nonequilibrium phonons is interpreted with the aid of estimates of some of the parameters of the electron-phonon system. We conclude that the observed decay is dominated by anharmonic breakup of low-frequency optical phonons, which have recently been seen with inelastic neutron scattering in the (41—54)-cm^{-1} phonon-energy range of these experiments. Lifetimes in the 10-ns range are obtained, consistent with some theoretical estimates.

I. INTRODUCTION

The development of high-frequency phonon spectroscopy with good spectral, spatial, and temporal resolution is of great interest as a solid-state probe. It can be utilized to study low-frequency excitations and the nature of surfaces and adsorbates on these surfaces. It is also of interest to study the dynamics of these phonons, thereby testing theories for anharmonic decay and phonon scattering, both in the bulk and at surfaces. One important technique for studying nonequilibrium phonon distributions is vibronic sideband phonon spectroscopy (VSPS), first utilized for this purpose with the $N3$ center in diamond[1] and the bound exciton in CdS,[2] and then developed with great sophistication by Bron and Grill[3] using Eu^{2+} in SrF_2 to obtain spectral, spatial, and temporal information about the transport and relaxation of phonons due to heat pulses across surfaces and through the bulk.

These previous examples utilized anti-Stokes emission VSPS to obtain information on the nonequilibrium phonon distributions. We extend this technique by using anti-Stokes absorption VSPS. We show that the utilization of fluorescence-detected absorption greatly enhances the sensitivity of the technique making possible in some systems a potential sensitivity to phonon occupation numbers of 10^{-6} or less with the preservation of excellent spectral, spatial, and temporal resolution.

We apply the technique to the host LaF_3. Detection is accomplished with anti-Stokes absorption VSPS using the $^3P_0$ state of Pr^{3+} while monoenergetic phonon distributions are obtained at 41 and 54 cm^{-1} through single-phonon relaxation among excited states of Er^{3+} ions. These monoenergetic phonon distributions evolve in time with decay times of 46 and 35 ns for 41- and 54-cm^{-1} phonons, respectively. We argue that these are dominated by decay of either low-frequency optical modes or the longitudinal-acoustic modes. From an analysis of these decay times, estimates of the phonon lifetimes are obtained.

In Sec. II we present the anti-Stokes absorption VSPS technique and examine its potential sensitivity and spectral, spatial, and temporal resolution. The experimental techniques and results are described in Sec. III. In Sec. IV we analyze these results and obtain estimates of the phonon lifetimes. Our conclusions are presented in Sec. V.

II. ANTI-STOKES ABSORPTION VIBRONIC SIDEBAND PHONON SPECTROSCOPY

Electronic transitions of an atom or ion in a solid consist of a zero-phonon line accompanied by vibronic sidebands which result from the simultaneous excitation or destruction of one or more phonons. The energy shift of the absorption or emission from the zero-phonon line determines the phonon energy Δ. The relative strengths of the phonon sidebands depend on the electron-phonon coupling and the phonon density of states. In emission, the intensity of the anti-Stokes sideband, shifted from the zero-phonon line (energy ϵ_0) by the phonon energy Δ, is[4]

$$I_{AS}^{\rm em}(\epsilon_0+\Delta)=CN(\Delta)[n(\epsilon_0+\Delta)+1]\sum_{\lambda}\rho(\Delta,\lambda)F(\Delta,\lambda)\ , \quad (1)$$

where em represents the emission, AS is the anti-Stokes sideband, $N(\Delta)$ and $n(\epsilon_0+\Delta)$ are, respectively, the phonon occupation number at phonon energy Δ and the photon occupation number at the emission energy $\epsilon_0+\Delta$, $\rho(\Delta,\lambda)$ is the phonon density of states at energy Δ and for polarization branch λ, and $F(\Delta,\lambda)$ is the electron-phonon coupling strength. For the Stokes (S) sideband intensity in emission[4]

$$I_S^{\rm em}(\epsilon_0-\Delta)=C[N(\Delta)+1][n(\epsilon_0-\Delta)+1] \times\sum_\lambda \rho(\Delta,\lambda)F(\Delta,\lambda)\ . \quad (2)$$

If $F(\Delta,\lambda)$ is independent of Δ and λ then the Stokes sideband at low temperature $[N(\Delta)\ll 1]$ and for low light intensities $[n(\epsilon_0\pm\Delta)\ll 1]$ maps out the phonon density of states.

The phonon occupation number at low temperatures $(\Delta\gg kT)$ can be obtained from the ratio of the anti-Stokes to Stokes emission intensities

$$N(\Delta)=\frac{I_{AS}^{\rm em}(\epsilon_0+\Delta)}{I_S^{\rm em}(\epsilon_0-\Delta)}\ . \quad (3)$$

This ratio reflects the instantaneous value of $N(\Delta)$ with an energy resolution which depends on the half-width of the zero-phonon line and/or the spectral resolution of the spectrometer analyzing the emission. If the excited ions responsible for the emission are produced in a small volume, for instance, by a laser, then high spatial resolution can also be achieved. Bron and Grill[3] utilized this technique to examine the spectral, spatial, and temporal evaluation of phonons in SrF_2 using phonon sidebands of Eu^{2+}.

These same ideas apply in absorption where the absorption coefficients (ab) are

$$\alpha_S^{\rm ab}(\epsilon_0+\Delta)=C'[N(\Delta)+1]n(\epsilon_0+\Delta)\sum_\lambda \rho(\Delta,\lambda)F(\Delta,\lambda) \quad (4)$$

and

$$\alpha_{AS}^{\rm ab}(\epsilon_0-\Delta)=C'N(\Delta)n(\epsilon_0-\Delta)\sum_\lambda \rho(\Delta,\lambda)F(\Delta,\lambda)\ . \quad (5)$$

Note that for absorption the Stokes process involves a photon whose energy exceeds that of the electronic origin, reflecting the fact that the Stokes process increases the energy of the medium. For anti-Stokes absorption the energy of the medium is decreased resulting in absorption of a photon whose energy is less than that of the electronic origin. At low temperatures we obtain

$$N(\Delta)=\frac{\alpha_{AS}^{\rm ab}(\epsilon_0-\Delta)}{\alpha_S^{\rm ab}(\epsilon_0+\Delta)}\ . \quad (6)$$

Consider a probe ion excited with a focused laser beam by absorption into the anti-Stokes phonon sideband of a fluorescing metastable state. At low temperatures where the equilibrium phonon occupation number $N(\Delta)$ is nearly zero, absorption can occur only in the presence of nonequilibrium phonons at energy Δ and its strength is proportional to $N(\Delta)$ as shown in Eq. (6). The absorption is obtained from the resulting total integrated emission which can yield very high sensitivity relative to anti-Stokes emission which can only utilize that part of the emission which occurs during the phonon lifetime, often much less than the radiative lifetime. The time of detection is the on-time of the pulsed probe laser, which is 5—8 ns in the present case, but which can be in the picosecond regime. The phonon energy is determined by the frequency shift of the laser from the zero-phonon line. The energy resolution is limited by a combination of the laser linewidth, which can be very narrow, and the homogeneous and inhomogeneous contributions of the excited-ion resonance width. In the present case the inhomogeneous linewidth dominates. In fluorescent detection of absorption, the spectral resolution of the spectrometer is unimportant and this fact greatly enhances the sensitivity of anti-Stokes absorption VSPS relative to anti-Stokes emission VSPS. The energy spectrum of the phonon distribution is obtained by sweeping the laser frequency on the low-frequency side of the zero-phonon line while the temporal evolution of the phonons is captured by varying the delay between the detector laser and the external event generating the nonequilibrium phonon distribution.

The main difficulty with anti-Stokes absorption VSPS is background fluorescence which can occur even in the absence of nonequilibrium phonons due to impurities, perturbed probe-ion sites, or multiphoton absorption. However, utilizing difference techniques for measuring the integrated emission intensity with and without the nonequilibrium phonons, this problem can be greatly diminished.

III. EXPERIMENTS

LaF_3 double doped with 0.05 at. % Pr^{3+} and 0.3 at. % Er^{3+} was utilized for these investigations. Rare earths in LaF_3 give sharp zero-phonon spectra with weak phonon sidebands. Pr^{3+} has a singly degenerate excited manifold, $^3P_0$ at 20 926 cm^{-1}, whose phonon sidebands have been studied.[5] The absence of any nearby electronic states simplifies the interpretation of the experiments. The $^3P_0$ state fluoresces strongly with a radiative lifetime of $\sim 50\ \mu$s. The probe ions were excited with a thyratron triggered N_2 laser pumping a tunable dye laser. It is important for these experiments to minimize the amplified spontaneous emission from the dye laser, as this, by virtue of its broadband nature, can resonantly excite some Pr^{3+} ions producing a background fluorescence. Therefore, a fraction of the N_2 laser was used to pump an oscillator, whose output was spectrally filtered through a 0.25-m monochrometer, with amplification occurring in a second dye cell pumped with the remainder of the N_2-laser output ($\sim 70\%$). The resulting 4-ns probe pulse contained $\sim 100\ \mu$J in a 0.5-cm^{-1} bandwidth using a grazing incidence grating-mirror combination in the oscillator cavity.[6]

Nonequilibrium phonons were obtained from the laser-excited Er^{3+} codopant ions. The second and third crystal-field states of the $^4F_{9/2}$ manifold have separations of $\Delta=41$ and 54 cm^{-1} relative to the lowest state.[7] A doubled Nd:yttrium aluminum garnet (Nd:YAG) laser was used to pump a pulsed tunable dye laser with two amplifiers yielding 6-ns, 10-mJ pulses with a bandwidth of 0.3 cm^{-1}. These tunable optical pulses from the source laser at frequency ν_S resonantly excited the second or third crystal-field levels of the $^4F_{9/2}$ manifold, as shown in Fig. 1, generating phonons at energy Δ via the subsequent single-phonon relaxation to the metastable state. The relaxation occurs rapidly relative to the temporal width of the laser so that the phonons are generated with

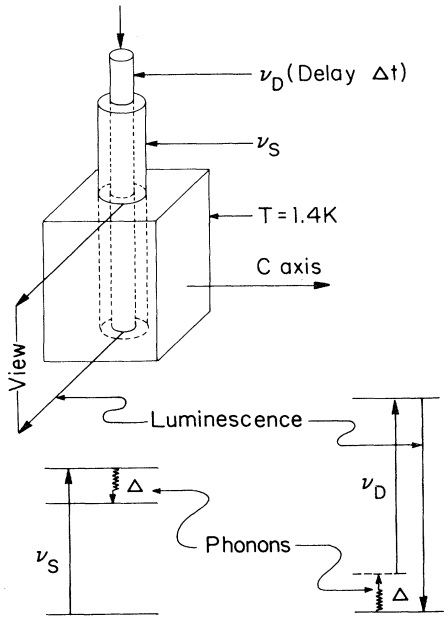

FIG. 1. Experimental arrangement showing overlap of source laser at frequency ν_S and detector laser at frequency ν_D (top figure) and the schematic energy-level structure of the impurity ions acting as the phonon source (lower left) and detector (lower right). The phonons are generated in the source at energy Δ by single-phonon emission and are detected using the luminescence resulting from the anti-Stokes absorption induced by the presence of phonons at Δ.

the temporal response of the Nd:YAG pumped dye laser.

The experimental geometry is shown at the top of Fig. 1. The phonon source laser illuminates a 2-mm-diam. cylinder within which is the detector laser beam. Luminescence is observed at right angles to the directions of the source and detector beams. Phonons of energy Δ are generated from single-phonon relaxation on the Er^{3+} sites as shown on the lower left-hand side of Fig. 1 and are detected by the luminescence resulting from the anti-Stokes absorption of the Pr^{3+} ions as shown on the lower right-hand side of Fig. 1.

The phonon detector laser was delayed relative to the source laser with a variable delay. Pr^{3+} luminescence to the 322-cm^{-1} crystal-field level of the ground state at 4852 Å was isolated with a 0.75-m Spex spectrometer with 400-μm slits. The luminescence was detected with an Amperex 56 TVP phonomultiplier whose output was stored on a Biomation 6500 transient digitizer. The output occurring during the first 20 μs was discarded as it contained some afterpulsing of the photomultiplier due to scattered laser light entering the spectrometer. The next 50 μs of the data were stored in the transient digitizer and were transferred to a multichannel scalar where the pulses were counted. The phonon-detector laser was fired at twice the frequency of the source laser. The number of detected photons with only the probe laser were stored in one channel of a multichannel scalar while the photons counted with both lasers were stored in a second channel. The absorption produced by the nonequilibrium phonons was obtained from the difference. The difference signal was normalized to the total integrated light intensity of the probe laser, obtained from the output of a photodiode recorded on an integrating digital voltmeter. The relatively small variation of the total energy output of the phonon source laser was ignored.

We first examined the Stokes and anti-Stokes absorption at $T=1.4$ K using the integrated fluorescence with only probe-laser excitation. This is shown in Fig. 2 for the π and σ polarizations of the detector laser. The Stokes absorption can be compared with the unpolarized absorption measurements in a 1 at.% LaF_3:Pr^{3+} sample made by Yen, Scott, and Schawlow.[5] They found the strongest sideband at about 55 cm^{-1}, with weaker peaks at about 150 and 170 cm^{-1}, in reasonable agreement with Fig. 2. A sharp peak at 26 cm^{-1} is not observed in our data. It probably arises from the same mechanism as that which produces sharp structure in our data on the anti-Stokes side and at 15 cm^{-1} on the Stokes side. The sharp line structure on the anti-Stokes side cannot be phonon induced at 1.4 K and probably indicates the presence of a large number of Pr^{3+} sites with nearby defects as has been seen by other workers.[8] The maximum Stokes sideband intensity at 55 cm^{-1} has an absorption which is about 10% of that of the zero-phonon line.

Spectra on the anti-Stokes side were then recorded by alternately exciting the sample with only the probe laser to obtain a background and both the phonon source and detector lasers. The spectrum with only the detector laser is shown in Fig. 3 by the open circles. The difference spectrum for a time delay between laser pulses of 15 ns is shown by the closed circles. This signal is proportional to

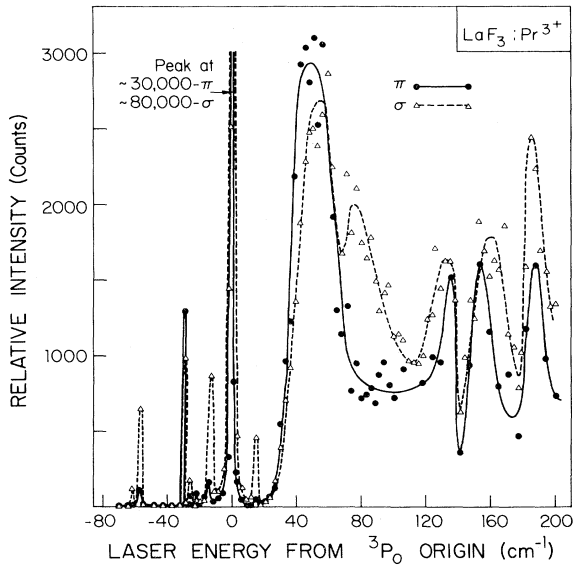

FIG. 2. Excitation spectrum near the $^3H_4 \rightarrow {}^3P_0$ Pr^{3+} zero-phonon line of 0.05 at.% LaF_3:Pr^{3+}. Fluorescence is detected from the $^3P_0 \rightarrow {}^3H_4$ (322-cm^{-1}) transition. Energy is measured relative to the zero-phonon transition. Phonon sidebands are observed on the Stokes side and absorption from perturbed Pr^{3+} ions is seen on the anti-Stokes side.

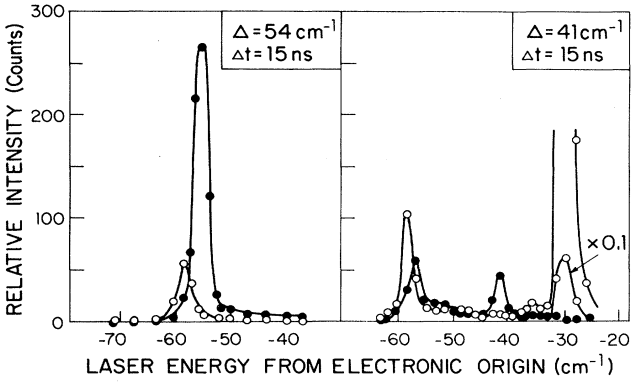

FIG. 3. Integrated blue luminescence from $Pr^{3+}(^3P_0)$ and difference luminescence signals. Open circles are obtained with only the detector laser at ν_D. Closed circles are obtained as the difference between the integrated blue luminescence with both ν_D and ν_S and with only ν_D. The difference signal is proportional to the phonon occupation number at energy Δ, selected by the amount by which the detector laser is tuned below the zero-phonon line.

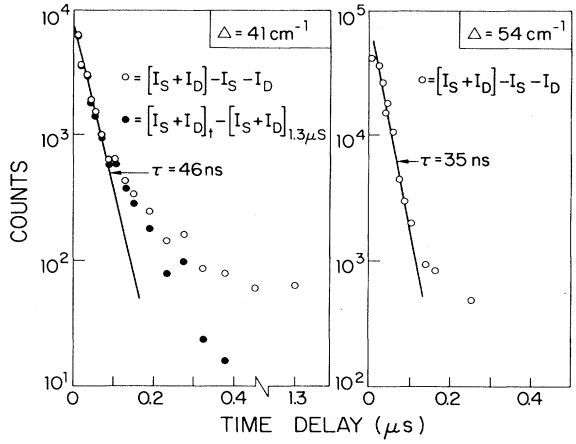

FIG. 4. Dependence of the phonon-induced Stokes absorption on delay between the phonon source and detector laser. The source laser is tuned to the $\Delta=41$ or 54 cm^{-1} excited Er^{3+} state, respectively. The detector laser is tuned below the zero-phonon line by the appropriate energy Δ. The open circles represent the difference in the integrated luminescence with both lasers present less the sum of the signal with each laser by itself. For the closed circles, the residual signal with both lasers present at delay time 1.3 μs is subtracted from the signal at delay time t.

the nonequilibrium phonon population 15 ns after phonon generation. The source laser was first tuned to the lowest-excited component of the $^4F_{9/2}$ manifold of Er^{3+}, producing 41-cm^{-1} phonons, while in the second case, absorption was tuned to the second excited component at 54 cm^{-1}. Clear peaks in the difference spectra was obtained at 41 and 54 cm^{-1}, depending on which of the Er^{3+} excited states was pumped, indicating generation and detection of these nonequilibrium phonons. The peak at 57 cm^{-1} in the difference spectrum for 41-cm^{-1} phonon excitation is probably a result of absorption from the first excited component of a $^3H_6$ ground-state manifold of Pr^{3+} which has a much larger absorption coefficient to $^3P_0$ than the absorption from the ground state. The source laser probably induces a small amount of heating, generating a broad band distribution of phonons which populate this 57-cm^{-1} state to a small degree (occupation number $<10^{-6}$). The difference signals may be compared quantitatively with the Stokes absorption of Fig. 2. Using Eq. (6), we see that the resulting nonequilibrium phonon occupation numbers are $\simeq 10^{-1}$ for the 54-cm^{-1} phonons and $\sim 2\times 10^{-2}$ for the 41-cm^{-1} phonons.

The peak in the difference signal disappears if the source laser is tuned off-resonance from the Er^{3+} absorption or if it is tuned to the lowest $^4F_{9/2}$ crystal-field state. The peak is also absent if the probe laser is fired prior to the source laser or if it is delayed by more than 1 μs relative to the source laser.

The temporal evolution of the nonequilibrium phonon population is shown in Fig. 4, which was obtained by fixing the probe-laser frequency 54 or 41 cm^{-1} below the zero-phonon $^3P_0$ resonance while the source-probe delay time was varied. The data represented by the open circles are the number of fluorescent counts obtained with the source and detector laser both present less the number of counts obtained with source and probe lasers independently. The data are nonexponential with small difference signals remaining after 1 μs. In the case of the 41-cm^{-1} phonons, this long-tail background was subtracted from the raw data yielding a more exponential decay. From the slope of the initial rapid decay over the first decade we obtain relaxation times of 35 and 46 ns for the 54- and 41-cm^{-1} phonons, respectively.

IV. ANALYSIS

In order to analyze the observed monochromatic phonon signals and understand their decay it is necessary first to estimate some of the essential parameters describing the phonon dynamics in this system. These include specific properties of the phonons in LaF_3 such as their dispersion relations, density of states (in each branch), and intrinsic elastic and anharmonic scattering lifetimes. In addition, it is important to know certain properties of the phonon interaction with the excited Er^{3+} ions used to generate the phonons, such as T_1^{-1}, the electron longitudinal relaxation rate, and τ_{res}^{-1}, the phonon scattering rate due to phonon absorption by the metastable excited Er^{3+} ions.

The phonon dispersion relations in LaF_3, recently obtained by Dixon and Nicklow,[9] are reproduced in Fig. 5. Note the low-frequency optical modes which extend over the two-phonon energies examined here (41 and 54 cm^{-1}). Because of their small bandwidth, we estimate that they in fact make the major contributions to the phonon density of states at 41 cm^{-1}. The TA and LA branches show little dispersion at 41 cm^{-1} while at 54 cm^{-1} the TA modes are quite near the zone boundary and are dispersive. Estimates for $\rho(\lambda,\Delta)$, the density of states at $\Delta=41$ and 54 cm^{-1}, are shown in the first column of Table I for the different modes λ.[10]

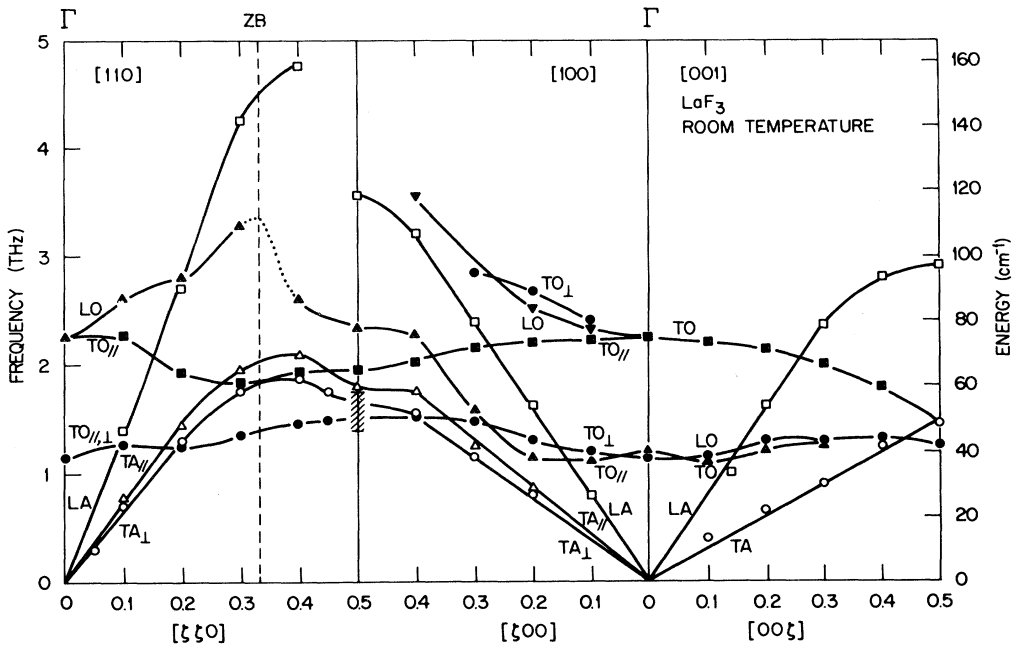

FIG. 5. Experimental dispersion curves for LaF_3 obtained by inelastic neutron scattering after Ref. 9.

As for intrinsic scattering processes, elastic scattering is unimportant as the phonons are strongly trapped by resonant scattering (see below). Inelastic processes are probably dominated by three-phonon anharmonic interactions whereby a phonon breaks up into two phonons conserving total energy and momentum. It will be argued that this is the main source for the decay of the observed phonons.

The spontaneous electron relaxation rate from the upper excited state responsible for the 41- or 54-cm^{-1} phonon generation can be estimated from homogeneously broadened optical linewidths of Pr^{3+} (Refs. 5 and 11) and Er^{3+} (Ref. 12) and temporal measurements on Ho^{3+} in LaF_3. These indicate that the relaxation rate T_1^{-1} is approximately proportional to Δ^5. We take the relaxation rate obtained from the measured homogeneously broadened linewidth of the $^4S_{3/2}(1)$ transition, terminating on the $^4I_{15/2}(2)$ state 51 cm^{-1} above the ground state of Er^{3+} in LaF_3 (Ref. 12) as the value for the 54-cm^{-1} state of $^4F_{9/2}$, i.e., 10^{11} s^{-1}, and scale by Δ^5 to obtain a value of 3.3×10^{10} s^{-1} for the 41-cm^{-1} state.

In the present case it is important to separate the contributions to T_1^{-1} from each of the three types of phonon modes resonant with the Er^{3+} excited-state energy splittings Δ. We note that the contribution from each phonon branch λ takes the form

$$T_1^{-1}(\lambda,\Delta) \propto |\langle 1|\mathcal{H}^{\lambda}_{e\text{-ph}}|2\rangle|^2 \rho(\lambda,\Delta) \tag{7}$$

TABLE I. Estimates of physical parameters used to interpret the phonon dynamics of LaF_3. We used $N^* = 3\times10^{18}$ cm^{-3} for construction of the table.

$\lambda(\Delta)$	ρ_λ $\left[\frac{\text{modes/cm}^3}{\text{cm}^{-1}}\times10^{19}\right]$	$\Sigma_\lambda(\Delta)$ $\left[\frac{\text{modes}}{\text{cm}^3}\times10^{19}\right]$	$T_1(\lambda,\Delta)$ (ps)	$\tau_{res}(\lambda,\Delta)$ (ns)	$\Lambda_\lambda(\Delta)$ (μm)
TA (41 cm^{-1})	5.2	2.1	330	2.3	6.5
LA (41 cm^{-1})	0.29	0.12	6000	2.3	13
O (41 cm^{-1})	37.5	15	46	2.3	0.7
Total (41 cm^{-1})	43.0	17.2	40		
TA (54 cm^{-1})	9	6.3	11.7	0.25	0.7
LA (54 cm^{-1})	0.5	0.35	210	0.25	1.5
O (54 cm^{-1})	1	0.7	105	0.25	0.7
Total (54 cm^{-1})	11.5	7.4	10		

and is proportional to the square of the electron-phonon matrix element coupling the two Er^{3+} excited states 1 and 2 and the phonon density of states $\rho(\lambda,\Delta)$ in branch λ. If we assume the matrix elements are identical, lacking any specific information on their relative properties, then

$$T_1^{-1}=T_1^{-1}(\mathrm{TA})+T_1^{-1}(\mathrm{LA})+T_1^{-1}(\mathrm{O}) , \tag{8}$$

where each term is proportional to the fractional contribution of $\rho(\lambda,\Delta)$ to the total density of states. Values of $T_1(\lambda,\Delta)$ are shown in column 3 of Table I.

The resonant scattering rate $\tau_{\mathrm{res}}^{-1}(\lambda,\Delta)$ is related to $T_1^{-1}(\lambda,\Delta)$ by[13]

$$\tau_{\mathrm{res}}^{-1}(\lambda,\Delta)=\frac{N^* T_1^{-1}(\lambda,\Delta)}{\Sigma_\lambda(\Delta)} , \tag{9}$$

where N^* is the excited Er^{3+} ion density, estimated as 3×10^{18} cm^{-3} at the site of the detector laser. From detailed balance it follows that τ_{res} is identical for all phonon branches at a given Δ since we have taken equal matrix elements. $\Sigma_\lambda(\Delta)$ is obtained from $\rho(\lambda,\Delta)$ through the expression

$$\Sigma_\lambda(\Delta)=\rho_\lambda(\Delta)d\Delta , \tag{10}$$

where $d\Delta$ is the resonant linewidth which is made up of a homogeneous and an inhomogeneous part. The homogeneous contribution is obtained from estimates of T_1^{-1} and is 0.2 and 0.5 cm^{-1} for the 41- and 54-cm^{-1} states, respectively. The inhomogeneous part is estimated as 0.2 cm^{-1}, about a factor of 3 or 4 less than the inhomogeneous optical linewidths observed in this material. This factor is typical of that observed in nonresonant fluorescent line-narrowing experiments.[11] The total excited-state resonance width is therefore estimated as 0.4 and 0.7 cm^{-1} for the 41- and 54-cm^{-1} states, respectively. The resulting estimates for $\Sigma_\lambda(\Delta)$ are shown in the second column of Table I and computed values of $\tau_{\mathrm{res}}(\lambda,\Delta)$ are listed in the fourth column. Note that estimates of $\tau_{\mathrm{res}}(\lambda,\Delta)$ are much less than the observed phonon-decay times.

Finally, we can estimate a mean free path $\Lambda_\lambda(\Delta)$ for resonant scattering

$$\Lambda_\lambda(\Delta)=v_{\lambda,\Delta}\tau_{\mathrm{res}}(\lambda,\Delta) , \tag{11}$$

where $v_{\lambda,\Delta}$ is the average phonon-group velocity of branch λ at energy Δ, measured as 2.8×10^5 and 5.8×10^5 cm/s for TA and LA phonons,[14] respectively, and estimated from the lowest-branch TO phonon dispersion curve as 0.3×10^5 cm/s for this mode.

Having obtained these parameters, we can calculate the initial phonon occupation number $N(\Delta)$ expected immediately after phonon generation. The number of phonons generated is identical to N^* as each excited ion produces a single resonant phonon. For $N(\Delta)\ll1$, $N(\Delta)$ is just $N^*/\Sigma_{\mathrm{tot}}\simeq0.018$ (41 cm^{-1}) and 0.04 (54 cm^{-1}) compared to observed values of 0.02 (41 cm^{-1}) and 0.1 (54 cm^{-1}). The good agreement is probably somewhat fortuitous given the uncertain estimates of $\rho(\lambda,\Delta)$ and $T_1^{-1}(\Delta,\lambda)$.

We can now interpret the observed phonon decays. The small values of $\Lambda_\lambda(\Delta)$ indicate strong resonant trapping of the phonons which therefore do not escape spatially from the volume excited by the source laser (2-mm diameter). Since $\tau_{\mathrm{obs}}(\Delta)$ the observed phonon decay satisfies the condition $\tau_{\mathrm{obs}}(\Delta)\gg\tau_{\mathrm{res}}(\lambda,\Delta)$, rapid mode conversion can occur at each reabsorption with a probability of conversion to another mode which is proportional to $\rho(\lambda,\Delta)$. Note that bottlenecking is unimportant here as $N^*/\Sigma_{\mathrm{tot}}\ll1$ so that the phonon energy does not spend a large amount of its existence as an electronic excitation.

In general,

$$\tau_{\mathrm{obs}}^{-1}(\Delta)=\sum_\lambda\frac{\Sigma_\lambda(\Delta)}{\Sigma_{\mathrm{tot}}}\tau_{\mathrm{anh}}^{-1}(\lambda,\Delta) , \tag{12}$$

where $\tau_{\mathrm{anh}}^{-1}(\lambda,\Delta)$ is the anharmonic decay rate for mode λ and energy Δ. Recent evidence, both experimental[4,15] and theoretical,[16] indicates that the lowest-frequency mode is long-lived. We will therefore assume that the near-zone-boundary TA modes are infinitely long-lived. The fact that we see no long-lived component to the observed decay, despite the fact that the TA modes make up a major fraction of the total phonon density of states, is consistent with the rapid mode-conversion hypothesis. We therefore set the term with $\lambda=\mathrm{TA}$ in Eq. (12) to zero. Noting from Table I that $\rho(\mathrm{O},41)\simeq130\rho(\mathrm{LA},41)$ we can set limits on the phonon lifetimes as shown by the following. *Case 1.* If $\tau_{\mathrm{anh}}^{-1}(\mathrm{O},41)\simeq\tau_{\mathrm{anh}}^{-1}(\mathrm{LA},41)$, then the density of states favor the LO and TO modes so that

$$\tau_{\mathrm{anh}}(\mathrm{O},41)\simeq\frac{\Sigma_{\mathrm{O}}(41)}{\Sigma_{\mathrm{tot}}(41)}\tau_{\mathrm{obs}}(41)\simeq40 \tag{13}$$

(measured in ns). *Case 2.* If, on the other hand, $\tau_{\mathrm{anh}}^{-1}(\mathrm{LA},41)\gg\tau_{\mathrm{anh}}^{-1}(\mathrm{O},41)$, then we have

$$\tau_{\mathrm{anh}}(\mathrm{LA},41)=\frac{\Sigma_{\mathrm{LA}}(41)}{\Sigma_{\mathrm{tot}}(41)}\tau_{\mathrm{obs}}(41)\simeq0.3 \tag{14}$$

(measured in ns). These conditions only set the limiting lifetimes consistent with Eq. (12). However, since one expects LA, TO, and LO phonons to have similar inelastic lifetimes for the same Δ,[17] we expect case 1 to be much more likely with $\tau_{\mathrm{anh}}(\mathrm{O},41)\simeq\tau_{\mathrm{anh}}(\mathrm{LA},41)\simeq40$ ns.

At 54 cm^{-1}, the LA and O modes make more nearly equal contributions to $\rho(\lambda,\Delta)$ so that we conclude either that

$$\tau_{\mathrm{anh}}(\mathrm{O},54)\simeq\tau_{\mathrm{anh}}(\mathrm{LA},54)\simeq5 \tag{15}$$

(measured in ns) or that one of these is ~3 ns and the other $\gg5$ ns.

Theoretically, estimates for $\tau_{\mathrm{anh}}(\mathrm{LA},\Delta)$ can be obtained in the limit of an isotropic dispersionless Debye solid based on either γ, the Grüneisen parameter, or on linear combinations of higher-order elastic constants. Unfortunately, neither of these parameters is known for LaF_3. With the use of a value of $\gamma=1$, the expression of Klemens[18] yields a lifetime of about 50 ns. Bron[19] has estimated the lifetime for 23-cm^{-1} LA phonons in LaF_3 based on reasonable values for the higher-order elastic constants. Scaling his result (600 ns) by Δ^{-5} yields values of 33 ns ($\Delta=41$ cm^{-1}) and 9 ns ($\Delta=54$ cm^{-1}). These values are close to the range of values obtained from the analysis of our experiments (see Table II).

TABLE II. Comparison of experimentally estimated lifetimes with theoretical estimates.

Δ (cm^{-1})	τ_{expt}	τ_{theor} (ns)
41	Case 1: 40 ns (LO,TO)	33
	Case 2: 0.3 ns (LA)	
54	5 ns (LA,LO,TO)	7

VI. CONCLUSIONS

We have demonstrated that luminescence detection of anti-Stokes absorption vibronic sideband phonon spectroscopy is a sensitive technique for detecting nonequilibrium phonons especially when used in conjunction with monochromatic phonon sources. The technique offers good spectral, spatial, and temporal resolution and generates and detects phonons in the bulk, avoiding problems with surface transport. Its main drawback is the need to place impurity ions in the sample for generation and detection.

We have measured the lifetimes of low-frequency optical phonons and/or the high-frequency acoustic phonons, and while the analysis is not totally unambiguous, we estimate anharmonic lifetimes of about ~ 40 and 5 ns at 41 and 54 cm^{-1}, respectively. These values are consistent with estimates of phonon lifetimes in this material.

A previous measurement of the lifetime of 23-cm^{-1} LA phonons in LaF_3 (Ref. 20) indicated a value of 15 ns, a factor of 40 less than theoretical estimates. Comparing the present results at 41 and 54 cm^{-1} with the experimental value obtained at 23 cm^{-1}, we do not find the strong dependence (Δ^{-5}) of the anharmonic lifetime on phonon energy predicted theoretically[18] and recently observed in CaF_2.[21]

ACKNOWLEDGMENTS

This work was supported by the U. S. Army Research Office, Durham, North Carolina under Contract No. DAAG29-82-k-0088. We thank G. S. Dixon and R. M. Nicklow for permission to use their unpublished neutron-diffraction data.

[1]M. J. Colles and J. A. Giordmaine, Phys. Rev. Lett. 27, 670 (1971).

[2]J. Shah, R. F. Leheny, and A. H. Dayem, Phys. Rev. Lett. 33, 818 (1974).

[3]W. E. Bron and W. Grill, Phys. Rev. B 16, 5303 (1977); 16, 5315 (1977).

[4]W. E. Bron, Rep. Prog. Phys. 43, 301 (1980).

[5]W. M. Yen, W. C. Scott, and A. L. Schawlow, Phys. Rev. 136, A271 (1964).

[6]M. G. Littman and H. J. Metcalf, Appl. Opt. 17, 2224 (1978).

[7]W. F. Krupka and J. B. Gruber, J. Chem. Phys. 39, 1024 (1963).

[8]J. C. Vial, R. Buisson, F. Madeore, and M. Poirier, J. Phys. (Paris) 40, 913 (1979).

[9]G. S. Dixon and R. M. Nicklow (unpublished).

[10]The estimates of $\rho(\lambda,\Delta)$ were obtained assuming a dispersionless, isotropic, Debye model. For the TA and LA branches velocities of sound obtained in Ref. 14 were used. For the optic modes, linear dispersion relations approximating those obtained experimentally (Fig. 5) were utilized. These were of the form $\omega=\omega_0+v_0k$ where ω_0 is the angular phonon frequency at $k=0$. The only optic modes which contribute at $\Delta=41$ cm^{-1} are the lowest LO and TO branches (assumed degenerate) for which we took $\omega_0=7.2\times10^{12}$ rad/s (38 cm^{-1}) and $v_0=0.32\times10^5$ cm/s. For $\Delta=54$ cm^{-1}, the situation is much more complicated as the lowest TO mode contributes along $\vec{k}||[\zeta 00]$ and the next lowest TO mode contributes along $\vec{k}||[00\zeta]$. Here the dispersion and anisotropy are far from negligible and it is meaningless to attempt a calculation of $\rho(O,54)$ without modeling the observed dispersion with a lattice-dynamics calculation which is beyond the scope of this paper. We therefore estimate a value $\rho(O,54)=2\rho(LA,54)=1\times10^{19}$ cm^{-3}.

[11]L. E. Erickson, Phys. Rev. B 11, 77 (1975).

[12]W. M. Yen, W. C. Scott, and P. L. Scott, Phys. Rev. 137, A1109 (1965).

[13]K. F. Renk and J. Peckenzell, J. Phys. (Paris) Colloq. 33, C4-103 (1972).

[14]C. Krischer, Appl. Phys. Lett. 13, 310 (1968).

[15]See, for example, R. G. Ulbrich, V. Narayanamurti, and M. A. Chin, Phys. Rev. Lett. 43, 1432 (1980); H. Lengfellner and K. F. Renk, J. Phys. (Paris) Colloq. 42, C6-259 (1981).

[16]M. Lax, P. Hu, and V. Narayanamurti, Phys. Rev. B 23, 3095 (1981). We note that the theorem proven in this reference forbidding the anharmonic decay of a phonon into phonons of higher phase velocity does not strictly apply to 41- and 54-cm^{-1} TA phonons in LaF_3 due to the presence of the low-frequency TO and LO branches. However, at 41 cm^{-1} there is very little phase space available in the lowest TO or LO modes into which a 41-cm^{-1} TA phonon could decay and in addition, the second phonon would of necessity have to be a low-frequency, small-$\vec{k}$ acoustic mode also of minimal phase space, resulting in long lifetimes. At 54 cm^{-1} a long anharmonic lifetime for TA phonons is more difficult to justify.

[17]P. G. Klemens, Phys. Rev. 148, 845 (1966).

[18]P. G. Klemens, J. Appl. Phys. 38, 4573 (1967).

[19]W. E. Bron, Phys. Rev. B 21, 2627 (1980).

[20]L. Godfrey, J. E. Rives, and R. S. Meltzer, J. Lumin. 18/19, 929 (1979).

[21]R. Baumgartner, M. Engelhardt, and K. F. Renk, Phys. Rev. Lett. 47, 1403 (1981).